Bull. Mater. Sci. (2019) 42:221
https://doi.org/10.1007/s12034-019-1907-0

© Indian Academy of Sciences

Evaluation of anticorrosive behaviour of ZnO nanotetra-pods on a AZ91-grade Mg alloy

R BRINDHA[1], S S RAJA AJITH[1], M NANDHINI[1], M SELVAM[1,*], KITTITAT SUBANNAJUI[2], KITTIKHUN KHOTMUNGKHUN[2] and K SAKTHIPANDI[3]

[1]Department of Nanoscience and Technology, K.S. Rangasamy College of Technology, KSR Kalvi Nagar, Tiruchengode 637215, India
[2]Material Science and Engineering Program, Multi-Disciplinary Unit, Faculty of Science, Mahidol University, Bangkok 73170, Thailand
[3]Department of Physics, Sethu Institute of Technology, Kariapatti 626115, India
*Author for correspondence (selvamic@gmail.com)

MS received 29 November 2018; accepted 2 April 2019

Abstract. Highly cross-linked zinc oxide (ZnO) with the nanorod morphology of tetra-pods was successfully prepared using a microwave irradiation (MWI) technique. In comparison with the available conventional techniques, the MWI technique has the advantage of producing different morphological structures with high purity and in a shorter reaction time. These tetra-pods consist of a ZnO core in the zinc blende from which four ZnO arms emerge in the wurtzite structure. In this investigation, the effects of irradiation times and the growth mechanism of ZnO nanotetra-pods were discussed. The structural, morphological and optical properties of ZnO nanorods were investigated by field emission scanning electron microscopy, X-ray diffraction, an ultra violet visible spectrometry and energy-dispersive spectroscopy. The electrochemical corrosion behaviours of an AZ91-grade Mg alloy and a ZnO/PN nanotetra-pod-coated Mg alloy were investigated. The Tafel plot revealed that the corrosion of Mg drastically decreased on coating with a thin layer of ZnO nanotetra-pods and PN (Mg/PN/ZnO) compared to Mg in a KOH electrolyte.

Keywords. Microwave irradiation; ZnO nanotetra-pods; structural properties; optical properties; corrosion studies.

1. Introduction

In recent years, semiconductors with one-dimensional (1D) nanostructures, such as rods, wires, belts and tubes have received attention due to their distinctive properties for applications in life-sciences and electronics [1–4]. It is known that 1D nanostructure is useful for investigations of electrical, thermal and mechanical properties, dimensionality and quantum confinement [5]. They play a significant role as both functional and structural units in the manufacture of microelectronic, electronic and electrochemical devices [6]. Recently, metal oxide nanoparticles with a morphology at a nanoscale <100 nm have become important [7]. Among these, zinc oxide (ZnO), an N-type semiconductor that has an extensive band gap of 3.37 eV and a large excitation binding energy of 60 meV at room temperature. ZnO is of research interest due to its unique properties [8]. ZnO nanostructures are used in catalytic reactions due to their higher catalytic activity and larger surface area [9]. ZnO nanoparticles with microstructures have been broadly used in gas sensors, transparent conductors and transistors, near-UV emission and piezoelectric applications [10–12]. ZnO nanoparticles have many applications in transparent electrodes [13], pH sensors [14], biosensors [15], UV photodiodes [16] and acoustic wave devices [17]. To date, a number of investigations have focussed on the production of ZnO nanoparticles through different methodologies, such as hydrothermal [18], sol–gel [19], electrochemical deposition [20] and vapour-phase process [21]. Previous studies on the synthesis of ZnO nanoparticles with a variety of morphologies, such as nanowires [22], nanorods [23], nanoneedles [24] and self-assembled architectures [25] have widely been reported.

ZnO nanotetra-pods were synthesized in this work using the microwave irradiation (MWI) technique at various durations of exposure. MWI is a type of heating method that has a number of applications in chemistry. Compared to conventional methods, such as hydrothermal [18], sol–gel [19], electrochemical deposition [20] and vapour-phase process [21], microwave (MW) synthesis has the advantage of producing smaller particle sizes with high purity owing to a short reaction time [26]. In the MWI technique, heat is generating internally within the material itself, instead of from an external source. Another benefit of the MWI technique is that there is no need for a post-annealing process [26]. These radiations have unique properties, such as homogeneous volumetric heating, which causes the heat to be directed directly

Published online: 28 June 2019

into the sample, which in turn leads to a high reaction rate, selectivity and increased product yield. In particular, MWs are electromagnetic radiations with frequencies that range from ∼500 MHz to 300 GHz. They are used in several technologies from mobile phones to satellites, and also in home appliances. Various systems depend on MW to transmit data; hence, MWI is still one of the greatest sustainable technologies for many industries. The advantage of ZnO prepared by the MWI technique is the production of smaller-sized particles with high purity owing to a short reaction time. The corrosion inhibition is better in ZnO nanotetra-pods prepared using MWI due to its high purity, smaller size and higher tetrapod formation possibility when compared to hydrothermal and sol–gel methods. The smaller size range of the prepared ZnO makes it to have higher surface area, and more number of surface atoms, thereby inhibiting more corrosive activity [27].

In this work, different nanostructure morphologies of ZnO were studied based on the time and power of MWI. The obtained ZnO nanostructures were characterized through X-ray diffraction (XRD), an ultraviolet (UV)–visible spectrophotometry, field emission scanning electron microscopy (FESEM) and energy-dispersive X-ray spectroscopy (EDX). Further, the ZnO nanotetra-pods prepared were coated onto a commercial magnesium alloy plate (AZ91) using the doctor blade technique [28,29]. Corrosion studies were carried out on a pristine Mg alloy plate and a ZnO nanotetra-pod-coated Mg alloy plate in KOH, NaCl and HCl electrolytes (three different electrolytes) using an electrochemical workstation (PGSTAT302N; Metrohm Autolab, The Netherlands). The influences of ZnO nanotetra-pods on the corrosion performance of Mg alloys were examined in detail.

2. Experimental

2.1 *ZnO nanotetra-pod synthesis*

A Zn ingot was bought from the automobile industry and made into Zn wool or Zn swarf by drilling. A Zn ingot with a weight of 7.8 kg was supplied by M/s Arrkay Engg Works, Chennai, India. A domestic MW oven (M/s Samsung ME711K), alumina crucibles, a sample container and ethanol were used as received, without further purification and changes. The synthesis of ZnO nanotetra-pods by the MWI method was carried out as shown in figure 1. Initially, 3 g of Zn swarf was added to an alumina substrate and placed in an MW oven. The substrate was then covered with an inverted alumina crucible and MW radiation was passed through the crucible. The swarf gets heated up as plasma and ejects the Zn atoms. The Zn atom oxidized and accumulated in the alumina crucible as shown in figure 2. In figure 2, the empty crucible before synthesis is shown on the left-hand side and the crucible with deposited ZnO nanorods is shown on the right-hand side. The time durations for exposure of MW radiation were 10, 20, 30, 60 and 90 s. The standard principle of this MWI method is that the

Figure 1. Pictorial representation of the preparation of ZnO nanotetra-pods.

Figure 2. ZnO nanotetra-pods collected in an alumina crucible.

Table 1. Chemical composition (weight %) of the AZ91 magnesium alloy.

Alloy	Mg	Al	Zn	Mn	Si	Cu	Ni	Fe
AZ91	90.012	9.0	0.7	0.24	0.04	0.005	<0.001	0.002

MW radiation induces an internal potential, which generates a very high field at the sharp peaks and edges of a metallic component (alumina foil) [30]. At these sharp peaks, electrons can excite and form a plasma arc. Hence, a sharp edge was needed to initiate ignition from the MW. This also explains why plasma can be ignited by irradiating a sharp swarf using MW. During the passage of MW radiation, air plasma sputtered Zn atoms were out of the swarf. Consequently, Zn atoms were oxidized and accumulated in the alumina crucible. The major compositions of air plasma are nitrogen and oxygen gases. The high-energy plasma is generally composed of ionized nitrogen atoms and ionized oxygen atoms, which can sputter Zn atoms out of the swarf. The products obtained from the MW air plasma were Zn vapours (deposition and floating fume), ZnO nanorods with the structure of tetra-pods, ozone

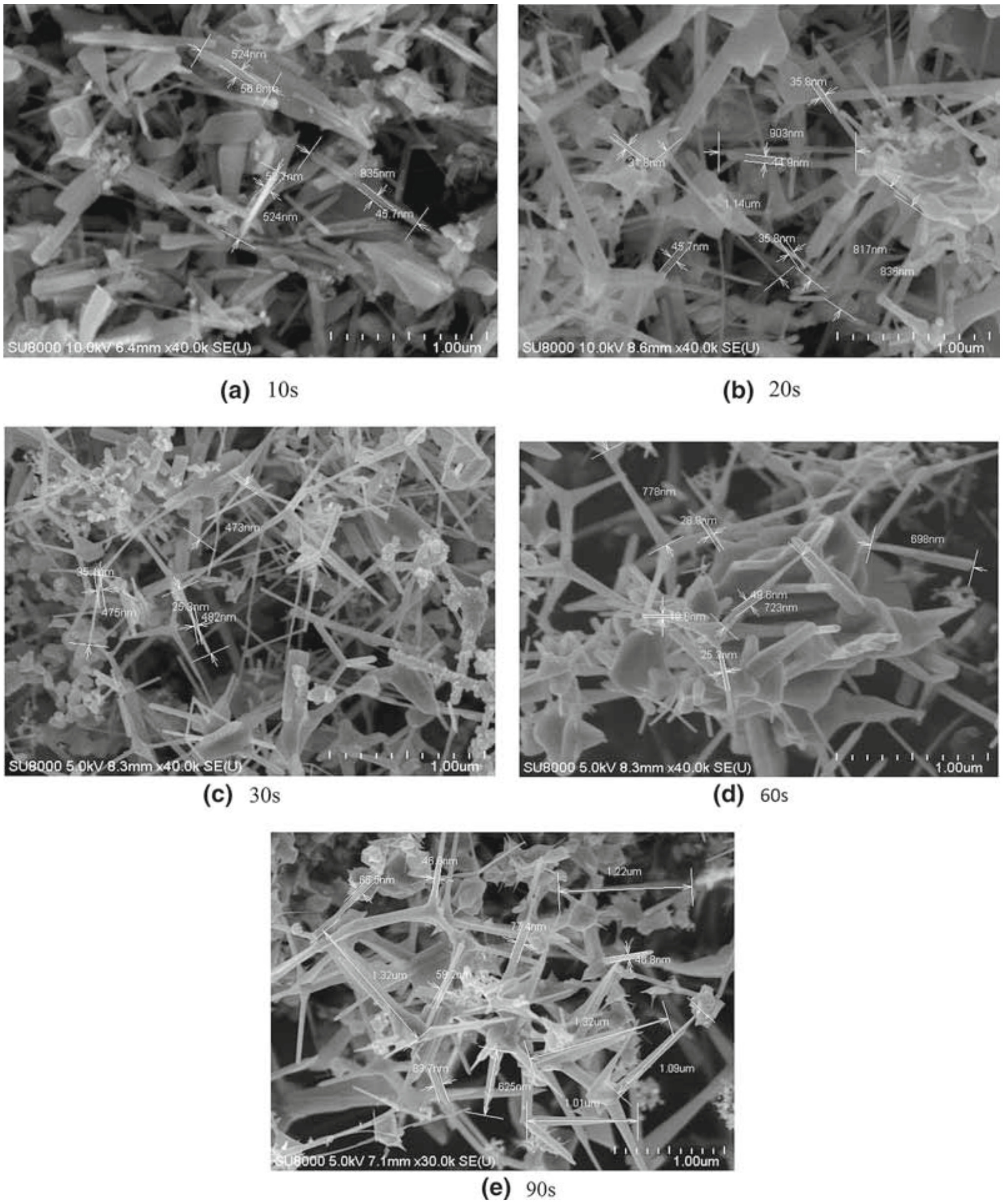

Figure 3. (**a**–**e**) FESEM image of synthesized ZnO nanotetra-pods at different time limits.

Table 2. Length and cross-sectional width of ZnO nanotetra-pods synthesized at different time limits.

S. no.	Time limit (s)	Length of rods	Cross-sectional width (nm)
1	10	470–490 nm	25–35
2	20	820–910 nm	30–50
3	30	800–900 nm	40–60
4	60	600–800 nm	15–50
5	90	610 nm–1.5 μm	40–90

Table 3. Yield of ZnO nanotetra-pods synthesized at different time limits.

S. no.	Time limit (s)	Yield of ZnO produced
1	10	350 mg
2	20	580 mg
3	30	920 mg
4	60	1.03 g
5	90	2.34 g

and nitrogen oxide. Nitrogen oxide and ozone were exhausted out of the hood, but deposited ZnO nanoparticles were collected inside the alumina crucible. Therefore, alumina was chosen because it has a high homogeneity of deposition compared with other substrates, such as glass and paper [31].

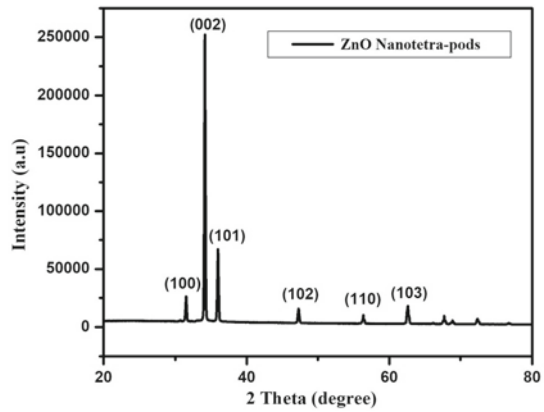

Figure 4. XRD pattern of ZnO nanotetra-pods prepared at 90 s.

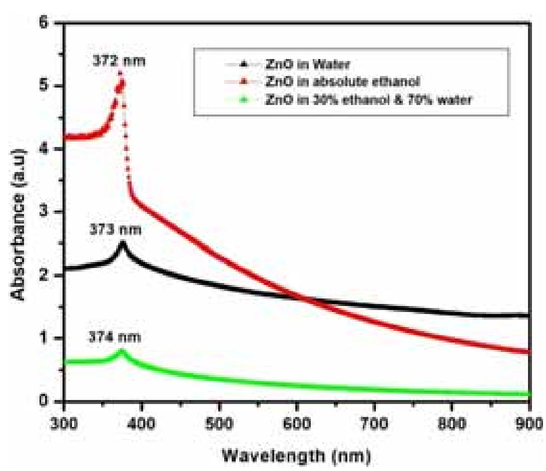

Figure 5. UV spectrum of ZnO nanotetra-pods prepared at 90 s.

2.2 *Material characterization*

The morphological structures of the synthesized nanoparticles at different time durations were studied through FESEM using a Hitachi SU8010 microscope. The microstructure was analysed by the XRD pattern using a Rigaku XtaLAB mini II, a benchtop X-ray crystallography system with a monochromatic CuKα 1 wavelength (λ) of 1.5406 Å. The average crystalline size (d) was determined using the Scherrer's formula: $d = k\lambda/\beta \cos\theta$, where k is the grain shape-dependent constant (∼0.9), θ is the Bragg reflection angle and β is the full-width at half-maximum of the main diffraction peak. The ultraviolet (UV) spectrum of the ZnO samples was recorded using a Shimadzu 1800 UV–visible DRS spectrophotometer. The elemental composition of ZnO was analysed using FESEM coupled with EDX (AMETEK, Z2E).

2.3 *Electrochemical corrosion studies: sample preparation*

An AZ91 magnesium metal plate was used for the present study. Table 1 shows the chemical composition (wt%) of the AZ91 magnesium alloy used for the present study. The metal plate was cut into a rectangular specimen (7.2 × 1.5 × 0.8 cm) and then, subsequently polished with 8, 6 and 1 mm silicon carbide grid papers and cleaned after each step with acetone. Initially, PVDF and N-methyl-2-pyrrolidone, hereafter denoted as PN with the weight ratio of 15:5 was prepared and coated separately on the Mg plate [32]. Further, the synthesized zinc oxide nanotetra-pods were also mixed with PN in the weight ratio of 80:15:5 and nanotetra-pods were coated again separately in a Mg plate using the doctor blade technique [28,29]. The coating was repeated three times to achieve a uniform thickness of ∼1 μm of PN and PN/ZnO measured using atomic force microscopy [33]. The coated-Mg metal was dried in a hot-air oven at 353 K for 1 h and then, used for corrosion studies. Hereafter, the coated-samples will be referred as Mg/PN and Mg/PN/ZnO.

2.4 *Electrochemical measurements*

The examination of corrosion characteristic behaviour in an Mg metal was performed using a three-electrode-cell set-up. In this cell set-up, an Mg metal was used as a working electrode, while platinum and saturated calomel were used as counter and reference electrodes, respectively. Electrochemical corrosion studies were carried out (until the concurrent value was obtained) for Mg, Mg/PN and Mg/PN/ZnO in different electrolytes (1 M KOH, 1 M HCl and 1 M NaCl) using the Autolab PGSTAT302N equipment (Metrohm Autolab, The Netherlands) [32]. The applied potential window for corrosion studies was 1.8–1 V at a scan rate of 5 mV s^{-1}. Corrosion potential (V_{corr}) and corrosion current (i_{corr}) were determined from the extrapolated data of the cathodic and anodic parts of the potentiodynamic polarization test or the Tafel plot. All these electrochemical measurements were performed three times to confirm the reproducibility of the results.

2.5 *Adhesion test*

To investigate the adhesion strength, a simple scotch tape test was performed on a PN–ZnO-coated AZ91 Mg plate. At room temperature, the pressure sensitive tape with adhesive nature is kept on the coated surfaces. To ensure good contact of the tape, the tape was rubbed firmly over the coated surface. The tape was then peeled by a pulling action at an angle of 90°. After the peeling of the tape, there exists three possibilities, namely, (a) the coated-film can be completely removed from the Mg plate, (b) the coated-film can not be removed at all and (c) the coated-film can be partly removed. Each test was repeated twice for conformity. The Scotch tape adhesion test was performed before and after corrosion (polarization) studies. Similarly, the weight loss data of the PN–ZnO-coated Mg plate were observed in HCl, KOH and HCl electrolytes as shown in table 5.

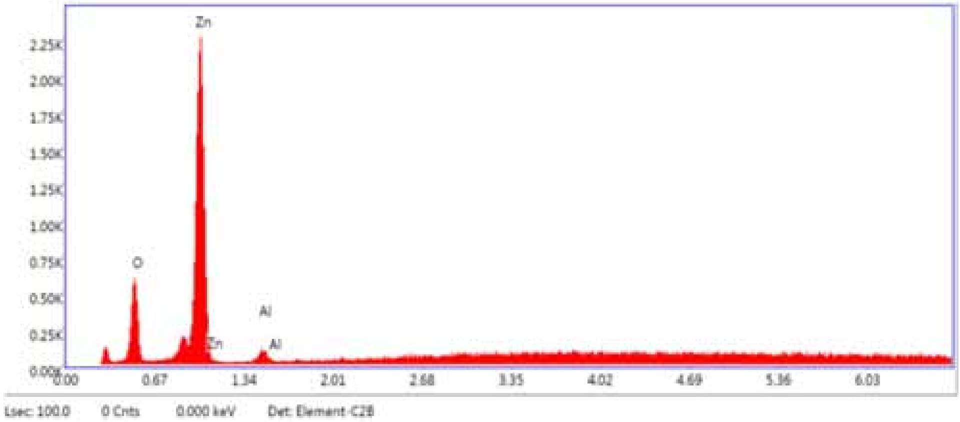

eZAF Smart Quant Results

Element	Weight %	Atomic %	Net Int.	Error %	Kratio	Z	A	F
O K	10.30	31.26	33.12	8.95	0.0680	1.3304	0.4957	1.0000
ZnL	87.67	65.09	160.66	3.14	0.8116	0.9584	0.9659	1.0000
AlK	2.03	3.65	4.84	21.57	0.0122	1.1717	0.5140	1.0004

Figure 6. Elemental composition of the synthesized ZnO sample by EDX prepared at 90 s.

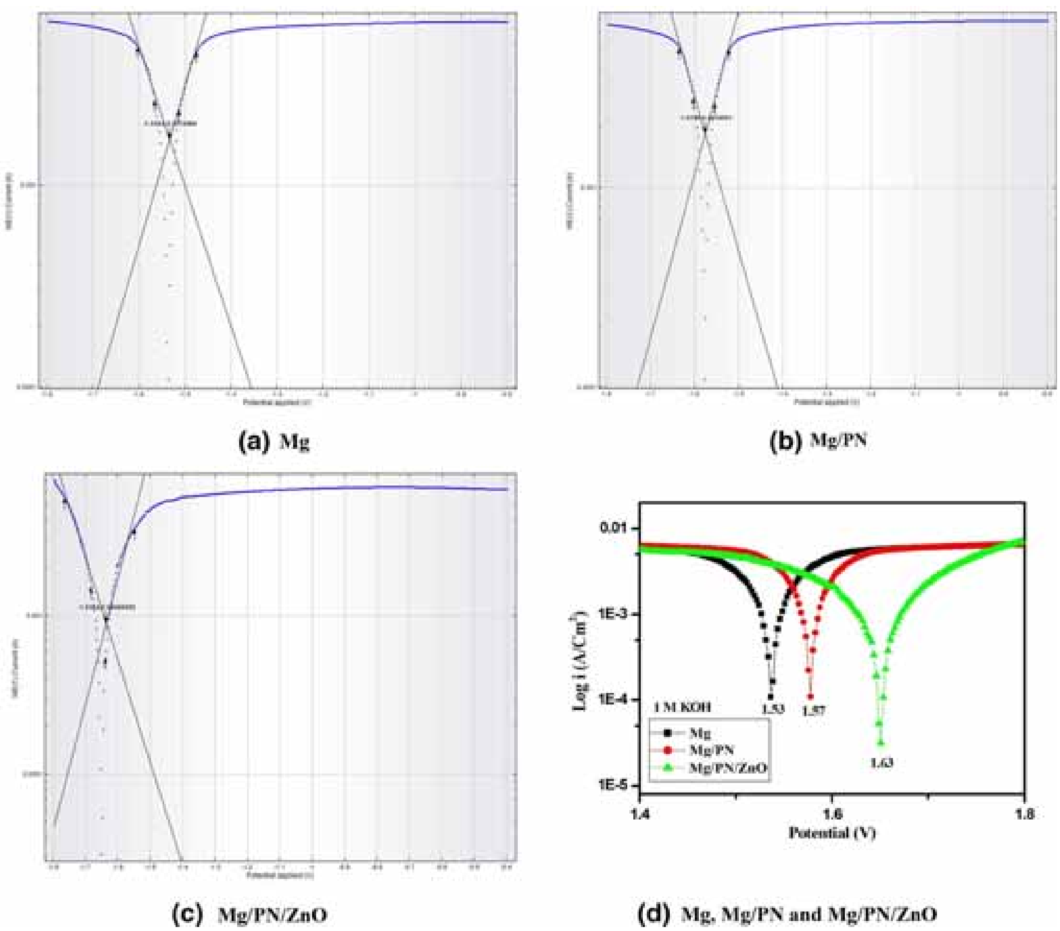

Figure 7. Potentiodynamic polarization curves for Mg, Mg/PN and Mg/PN/ZnO in a KOH electrolyte.

Table 4. Corrosion potential (V_{corr}) and corrosion current (i_{corr}) determined from Tafel curves of 1 M KOH, 1 M NaCl and 1 M HCl electrolytes.

Electrolyte	Sample	Corrosion potential (*vs*. SCR.E.) V^{-1}	Corrosion current (A cm^{-2}) $\times 10^4$
1 M KOH	Mg	1.53	1.68
	Mg/PN	1.57	1.85
	Mg/PN/ZnO	1.63	8.95
1 M NaCl	Mg	1.30	0.011
	Mg/PN	1.34	0.011
	Mg/PN/ZnO	1.49	1.50
1 M HCl	Mg	1.51	3.41
	Mg/PN	1.52	4.67
	Mg/PN/ZnO	1.59	8.65

3. Results and discussion

3.1 *Micro-structural studies*

The morphological characteristics of ZnO nanotetra-pods for different time durations are shown in figure 3a–e. These tetra-pods comprised a core ZnO in Zn blende from which four ZnO arms emerged in the wurtzite structure [34]. An increase in the equivalent dimensions of tetra-pods with an increase in the duration of synthesis was observed. From figure 3e, it is clear that each arm is well faceted with a hexagonal cross-section and is non-uniform in length and diameter. Generally, the growth of the cylindrical supports proceeds with the nucleation of a core assembly [35,36]. By varying the

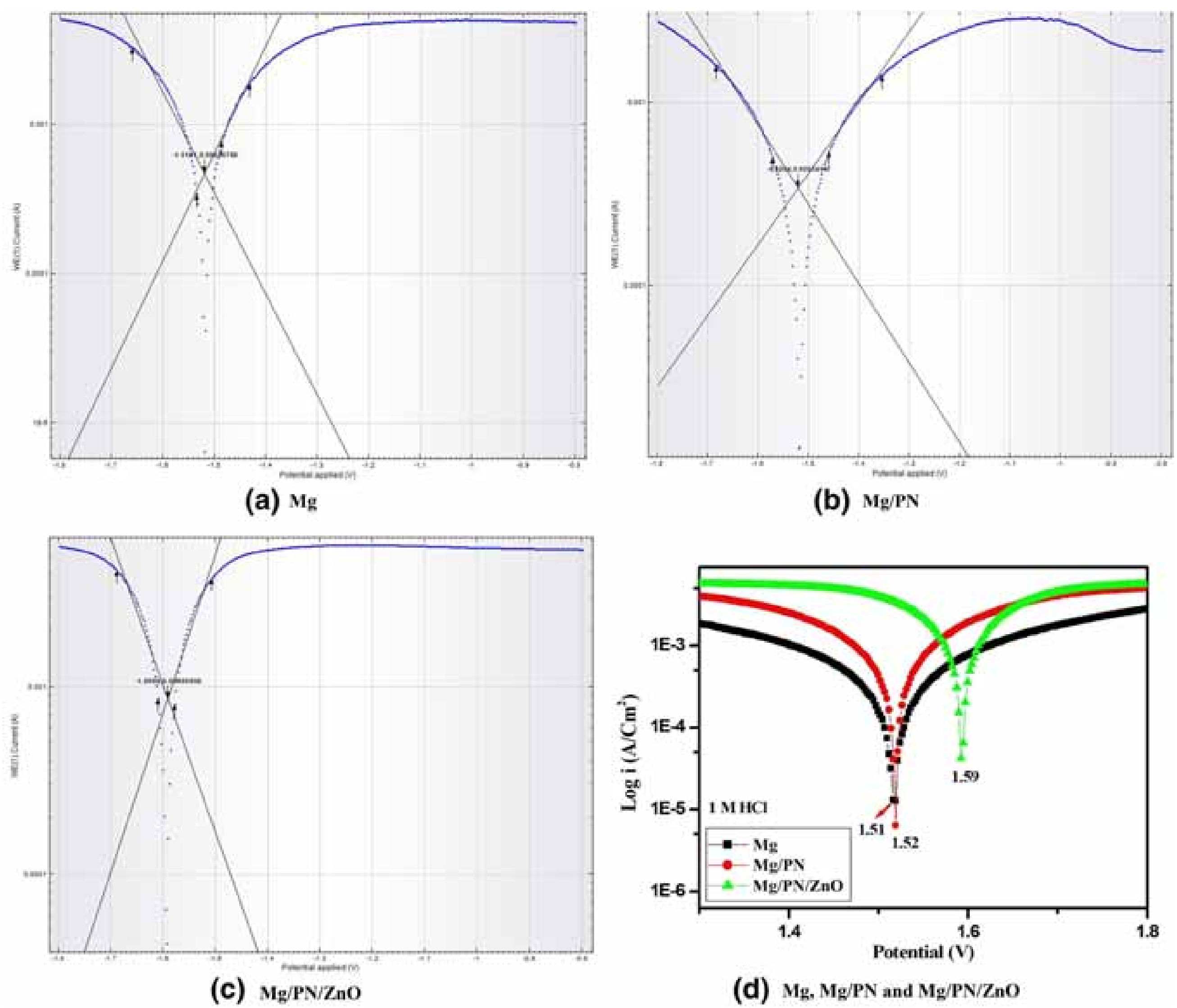

Figure 8. Potentiodynamic polarization curves for Mg, Mg/PN and Mg/PN/ZnO in a HCl electrolyte.

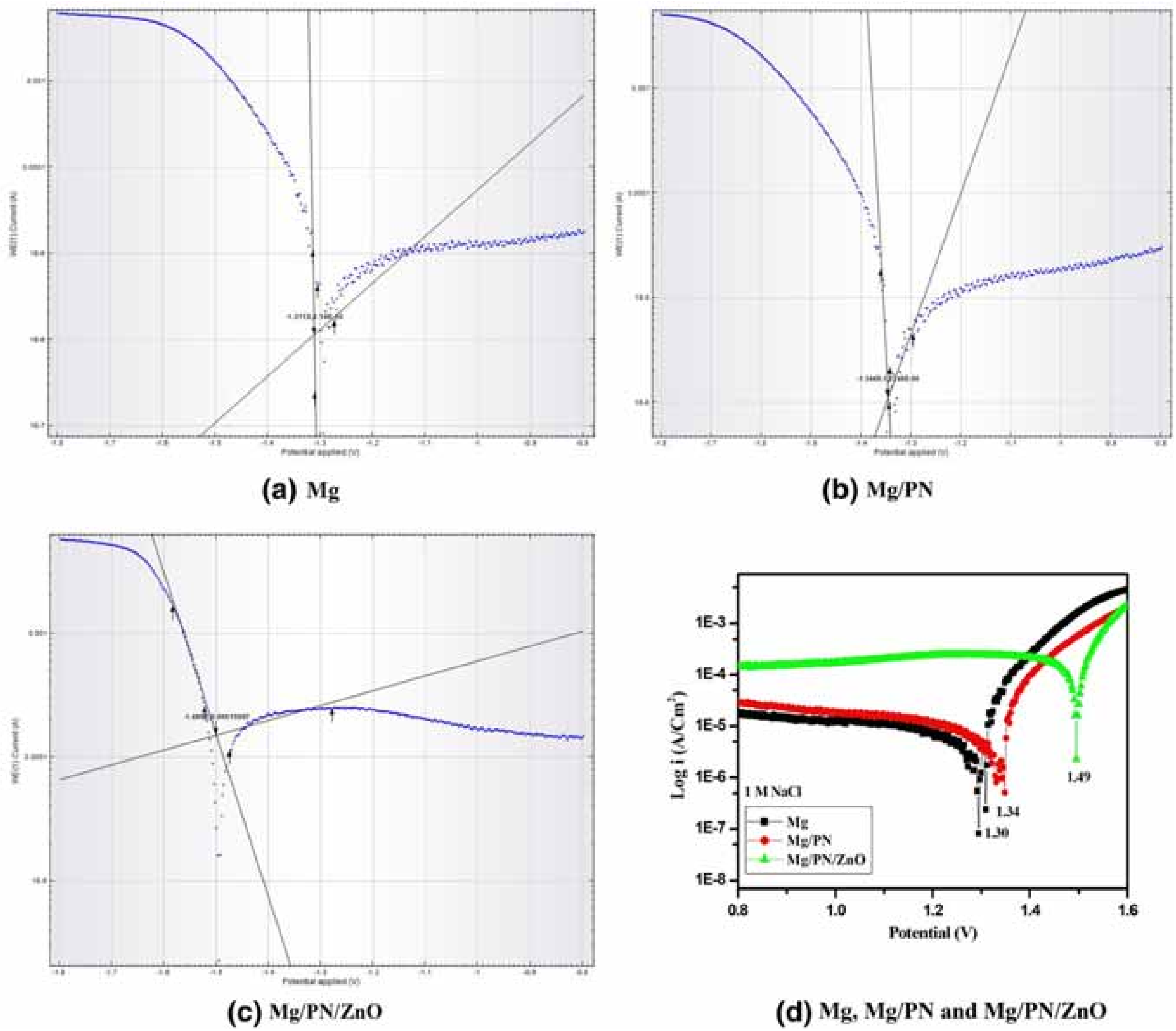

Figure 9. Potentiodynamic polarization curves for Mg, Mg/PN and Mg/PN/ZnO in a NaCl electrolyte.

growth parameters, such as the O_2 content and the MWI time duration, the morphology and the size of nanotetra-pods can be manipulated. We synthesized non-uniform tetra-pods with varying arm lengths and cross-sectional widths, as shown in table 2, by varying the growth conditions. One key advantage of tetra-pods over other nanocrystalline geometries is that they actively orientate with one arm directed normal to the plane of the Al substrate [34]. It is evident from figure 3a–e and table 2 that tetra-pods with high length to thickness ratios were obtained with the data synthesis duration of 90 s. Higher yields of tetra-pods were also observed at a synthesis duration of 90 s, and these are shown in table 3. On this basis, hereafter, for all the studies, ZnO nanotetra-pods synthesized over duration of 90 s are used.

The XRD pattern of ZnO shown in figure 4 confirms the suitable phase formation and the crystalline nature of the prepared ZnO nanotetra-pods at 90 s. The highest (002) intensity peak with other smaller intensity (100), (101), (102), (110) and (103) peaks of ZnO was observed in the XRD pattern. The crystallite size of ZnO nanotetra-pods was found to be 58.60 nm, which was calculated using the Scherrer's formula from the XRD pattern. In figure 4, the indexed diffraction planes represent the wurtzite phase of ZnO with the lattice parameters $a = 3.2492$ Å, $c = 5.2042$ Å and c/a ratio $= 1.612$, which are in agreement with the values reported in the literature ($a = 3.250$ Å, $c = 5.206$ Å, JCPDS no. 36-1451).

For the UV–visible absorption measurement, the ZnO nanotetra-pods prepared at 90 s were ultrasonically dispersed

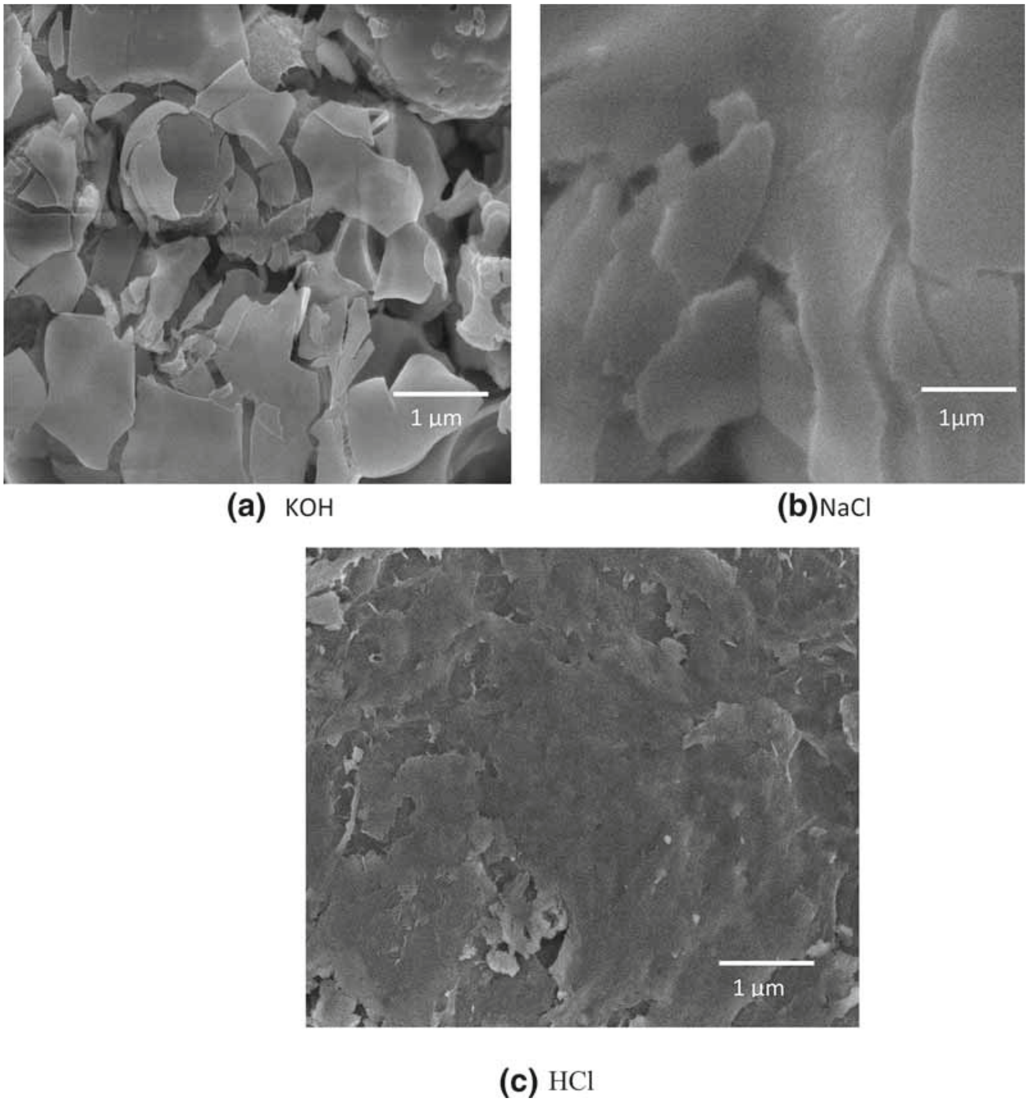

Figure 10. SEM images of Mg samples in three different electrolytes after corrosion studies.

in solvents, such as water, absolute ethanol and ethanol (30% in 70% double-distilled (DD) water). Before examination of the prepared powder, the spectrum was standardized for the solvent contribution (absolute ethanol, water and ethanol) and background. The absorption spectrum of ZnO nanotetra-pods with different solvents is shown in figure 5. It is clear that the spectrum has a well-defined excitation band at 373 nm with water as a solvent (corresponding band gap of ~3.32 eV). It is noteworthy that the wavelength is almost the same as the bulk absorption (373 nm) [37]. The absorption spectrum of ZnO nanotetra-pods in absolute ethanol as a solvent has an absorption band at 372 nm, which is red-shifted by −1 nm relative to bulk absorption at 373 nm. But this shift by −1 nm is very small; therefore, it will not alter the absorbance range. The reason for the shift of the absorption band could be the oriented attachment of the nanoparticles by MWI, which leads to the formation of defects in nanorods. Similar interpretations for fluctuations of absorption bands of ZnO towards the visible region have also been reported earlier [38]. The absorption spectrum of ZnO nanotetra-pods in ethanol (30% in 70% DD water) as a solvent is shown in figure 5 with an absorption peak at 374 nm.

The EDX spectrum of the ZnO nanotetra-pods at 90 s is shown in figure 6 which confirms the presence of Zn, O and Al in the prepared sample. The presence of a small amount of Al contamination from the alumina substrate (as expected) was observed along with the predominant Zn and O peaks. The EDX spectrum shows that the percentage of error for Zn is very low, which confirms the occurrence of Zn and O in the sample. The atomic percent ratio of O and Zn in the dried sample was, respectively, 31.26 and 65.09, which indicates that there were very few O_2 vacancy defects on the surface of the sample. Thus, the purity of the prepared ZnO was confirmed.

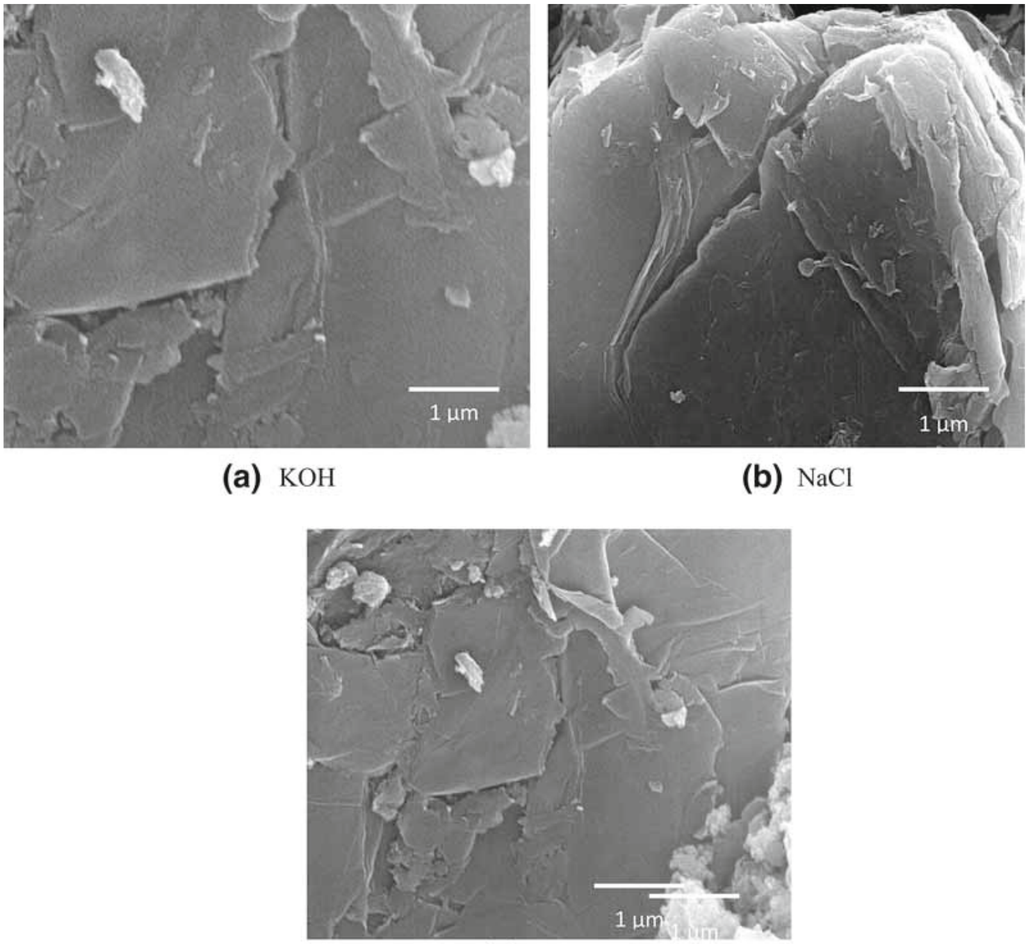

(a) KOH (b) NaCl (c) HCl

Figure 11. SEM images of Mg/PN samples in three different electrolytes after corrosion studies.

3.2 *Corrosion studies*

Comparative corrosion characteristics were studied for both the Mg alloy (Mg), Mg/PN and zinc oxide nanotetra-pod-coated Mg/PN alloy (Mg/PN/ZnO) samples in KOH, HCl and NaCl electrolytes. First, the potential was applied at 1.8 V and the corrosion was initiated at the Mg anode. Further, the potential tended to trace towards 1 V with an interval of $\sim$5 mV s^{-1}. Figure 7a–d shows the potentiodynamic polarization curves or Tafel plots for Mg, Mg/PN and Mg/PN/ZnO samples in 1 M KOH electrolyte solution. It is clear from figure 7a–d that the corrosion potential of the Mg/ZnO sample is moved towards more positive value (1.63 V) (anodic region) for Mg/PN/ZnO compared to Mg/PN (1.57 V) and Mg (1.53 V). The calculated corrosion current (i_{corr}), tabulated in table 4, was found to be $\sim$1.68 $\times 10^4$, $\sim$1.85 $\times 10^4$ and 8.95 A cm^{-2} for Mg, Mg/PN and Mg/PN/ZnO samples, respectively. The above results confirmed that a low rate of corrosion and high electrochemical corrosion resistance were achieved by a thin-layer coating of ZnO nanotetra-pods over the Mg anode surface.

Figure 8a–d shows the corrosion curves for Mg, Mg/PN and Mg/PN/ZnO in 1 M HCl electrolyte. A similar corrosion trend was observed. The corrosion current (i_{corr}) of Mg/PN/ZnO ($\sim$8.65 $\times 10^4$ A cm^{-2}) had a higher value than those of Mg/PN ($\sim$4.67 $\times 10^4$ A cm^{-2}) and Mg (3.41 $\times$ 10^4 A cm^{-2}). It is clear from figure 8a–d that the corrosion potential of the Mg/PN/ZnO sample is shifted towards more positive (1.59 V) (anodic region) value compared to Mg/PN (1.52 V) and Mg (1.51 V).

The corrosion curve for Mg, Mg/PN and Mg/PN/ZnO samples in 1 M NaCl electrolyte is plotted in figure 9a–d. It was also obvious that the Mg/PN/ZnO sample had higher corrosion current compared to the Mg/PN and Mg alloy sample, which suggests that improved corrosion resistance was achieved with the coating of ZnO nanotetra-pods over the Mg/PN and Mg surface. The Tafel slope was observed to be at a low potential for Mg and Mg/PN compared to Mg/ZnO, which also suggests a high corrosion rate for Mg. The calculated corrosion current (i_{corr}) of the Mg, Mg/PN and Mg/PN/ZnO samples was mapped from the extrapolated lines of the Tafel curve, table 4, and was ($\sim$0.01$\times 10^4$ A cm^{-2}),

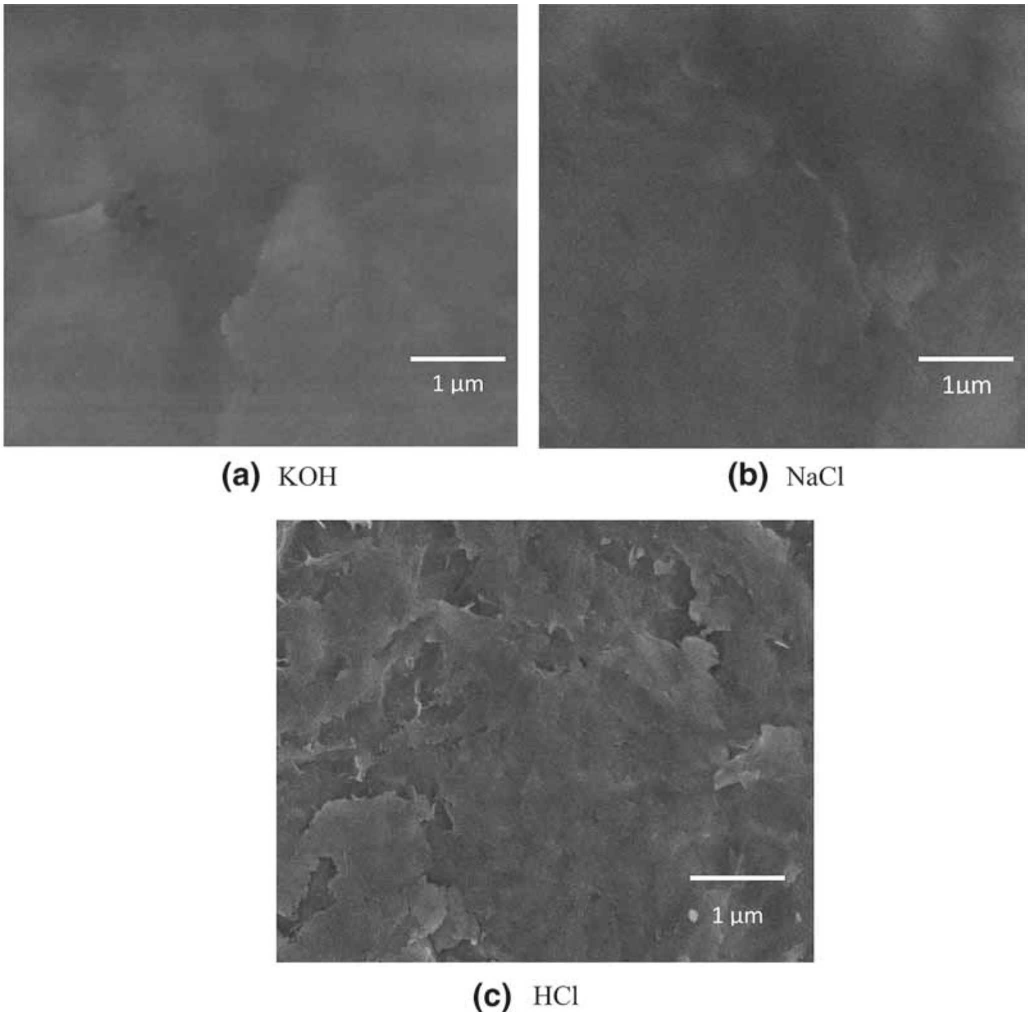

Figure 12. SEM images of Mg/PN/ZnO samples in three different electrolytes after corrosion studies.

($\sim 0.01 \times 10^4$ A cm^{-2}) and ($\sim 1.50 \times 10^4$ A cm^{-2}), respectively. It is clear from figure 9a–d that the corrosion potential of the Mg/PN/ZnO sample is moved towards more positive (1.50 V) (anodic region) value compared to Mg/PN (1.34 V) and Mg (1.30 V). The above experimental evidence confirmed that the ZnO thin-layer coating over the Mg and Mg/PN surface could improve corrosion resistance in aqueous electrolytes [39].

Figure 10a–c shows the degradation of the entire surface of the Mg alloy. This is because of constant surface corrosion and subsequent exposure to the positive potential in the electrolytes. Figure 11a–c also shows the degradation of the entire surface of the PN-coated Mg alloy. However, the surface of the Mg/PN/ZnO samples remained intact as shown in figure 12a–c, except for degradation in a few inaccessible areas with the majority of the sample surface unharmed. It is evident from the post-corrosion SEM study that ZnO nanotetra-pods do not corrode on the potential window used in our study. The above observation once again indicates that ZnO nanotetrapod-coated Mg (Mg/PN/ZnO) samples show high corrosion resistance. In addition, to support the above claim of considering Mg/PN/ZnO as a corrosion resistance material, weight loss data up to 6 h in KOH, HCl and NaCl electrolytes are noted in table 5. The initial weight of the Mg plate before coating PN/ZnO was 10.346, 10.975 and 10.847 g observed in KOH, HCl and NaCl electrolytes, respectively. Five-hundred milligrams of PN/ZnO was coated above the Mg plate and left for 6 h. At the end of each hour, the plates were dried for 10 min in a hot air oven at 120°C and the weight of the plates was measured using a weighing balance. Finally after 6 h, the weight of the Mg plate was 10.407, 10.975 and 21.848 g in KOH, HCl and NaCl electrolytes, respectively; the weight loss data for ZnO are shown in table 5. This implies that the weight loss of the PN/ZnO-coated Mg plate is minimum in the KOH electrolyte.

3.3 *Adhesion strength*

Adhesion plays a major role in determining the durability of the coated-films. The coated-films in three electrolytes (HCl,

Table 5. Weight loss data of the PN/ZnO-coated Mg plate.

		Weight loss of Mg plate (g) and ZnO (g) in three different electrolytes					
S. no.	Conditions	KOH	ZnO (g)	HCl	ZnO (g)	NaCl	ZnO (g)
1	Before coating PN/ZnO	10.346	—	10.975	—	10.847	—
2	After coating PN/ZnO	10.842	0.0	11.476	0.0	11.347	0.0
3	After coating PN/ZnO left for 1 h	10.712	0.13	11.368	0.108	11.243	0.104
4	After coating PN/ZnO left for 2 h	10.697	0.015	11.288	0.08	11.119	0.124
5	After coating PN/ZnO left for 3 h	10.607	0.09	11.197	0.091	11.039	0.08
6	After coating PN/ZnO left for 4 h	10.457	0.15	11.117	0.08	10.936	0.103
7	After coating PN/ZnO left for 5 h	10.437	0.02	10.977	0.14	10.856	0.08
8	After coating PN/ZnO left for 6 h	10.407	0.03	10.975	0.002	10.848	0.008

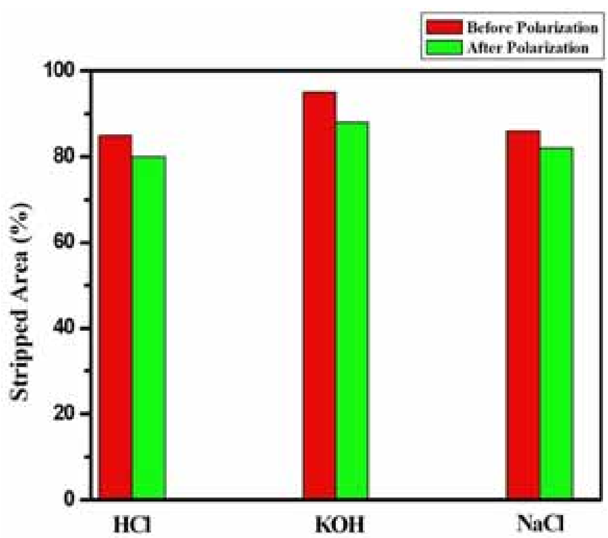

Figure 13. Adhesion strength of PN/ZnO coated on the Mg AZ91 Mg alloy on three different electrolytes before and after polarization.

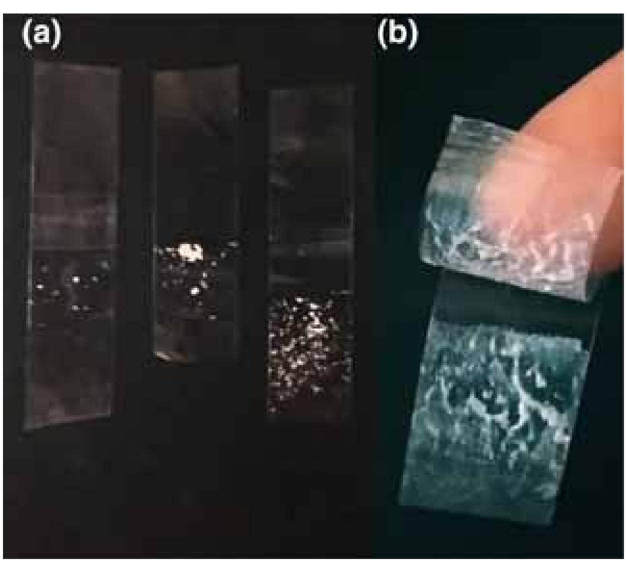

Figure 14. The Scotch tape test showing 0–5% removal of ZnO from the Mg plate.

KOH and NaCl) showed a 4B (0–5%) peel-off rate confirmed from ASTM standards, signifying small flakes of the coating are detached at intersections; <5% of the area is affected [40], which implies good adhesiveness and durability towards the Mg surface showed in figures 13 and 14. This adhesive strength was assumed to be the strong intercalation of ZnO on the polymer PVDF matrix. The ZnO nanotetra-pods showed good adhesive strength by means of fewer coated-surface peel off from the entire coated-surface.

4. Conclusion

In summary, ZnO can be synthesized by an energy-efficient, cost-effective and rapid MWI technique. To avoid corrosion in aqueous electrolytes, the prepared ZnO nanotetra-pods were applied as a thin-layer coating over an Mg alloy surface. Electrochemical measurements in three different aqueous electrolytes of KOH, NaCl and HCl showed a sharp decrease in the corrosion rate. The excellent corrosion resistance in aqueous electrolytes indicates that Mg/PN/ZnO can potentially be used as an anode material for a primary Mg battery system.

Acknowledgements

One of the authors, M Selvam, is grateful to the Department of Science and Technology (DST), New Delhi, for providing the INSPIRE fellowship (IF110749) to carry out this research work.

References

[1] Ram M K, Stefanakos E K and Yogi Goswami D 2013 *Mater. Sci. Semicond. Process.* **16** 2070
[2] Witte F, Hort N, Vogt C, Cohen S, Kainer K U, Willumeit R *et al* 2008 *Curr. Opin. Solid State Mater. Sci.* **12** 63
[3] Aochekpe N, Olorunfemi P O and Ngwuluka N C 2009 *Trop. J. Pharm. Res.* **8** 265

[4] Erdem Alaca B 2013 *Int. Mater. Rev.* **54** 245
[5] Toranzos V J, Portiz G, Luis Mochan W and Zerbino J O 2017 *Mater. Res. Express* **4** 1
[6] Selvam M, Srither S R, Saminathan K and Rajendran V 2016 *J. Ion.* **9** 1622
[7] Paula D R and Robeson L M 2008 *Polymer* **49** 3187
[8] Janotti A and Van de Walle C G 2009 *Rep. Prog. Phys.* **72** 1
[9] Fouad O A, Dai Q, Khader A E R S and Samy Ei-shall M 2011 *J. Nanopart. Res.* **13** 7075
[10] Zhu L and Zeng W 2017 *Sens. Actuators A* **267** 242
[11] Dahiya A S, Opoku C, Sporea R A and Sarvankumar B 2016 *Sci. Rep.* **6** 19232
[12] Opokua C, Dahiyaa A S, Oshman C, Cayrela F, Poulin-Vittrant G, Alquiera D *et al* 2015 *Phys. Proc.* **70** 858
[13] Ellmer K 2014 *Nat. Photonics* **6** 809
[14] Mani G K, Morohoshi M, Yasoda Y, Yokoyama S, Kimura H and Tsuchiya K 2017 *ACS Appl. Mater. Interfaces* **9** 5193
[15] Shiryaev M A, Eremin S A and Baranov A N 2014 *Nanotechnol. Russ.* **9** 99
[16] Chen H and Fang X 2015 *Mater. Today* **18** 493
[17] Hongsitha N, Wongrata E, Kerdcharoen T and Choopuna S 2010 *Sens. Actuators B* **144** 67
[18] Cao Z, Wang Y, Li Z G and Yu N 2016 *Nanoscale Res. Lett.* **11** 347
[19] Hasnidawani J N, Azlina H N, Norita H, Bonnia N N, Ratim S and Ali E S 2016 *Proc. Chem.* **19** 211
[20] Meng Y, Lin Y and Lin Y 2014 *Ceram. Int.* **40** 1693
[21] Abduev A K, Shasvarov A, Akhmedov A K and Terukov E I 2002 *Tech. Phys. Lett.* **28** 952
[22] Cuellar Murilloa G A, Bojorgea C D, Herediaa E A and Walsoe de Recaa N E 2015 *Proc. Mater. Sci.* **8** 630
[23] Yi G-C, Wang C and Park W I 2005 *Semicond. Sci. Technol.* **20** 22
[24] Qurashi A 2013 *J. Phys. Chem. Solids* **74** 166
[25] Liu Y, Li S, Lv H, Ping D, Li S, Li Z *et al* 2014 *Ceram. Int.* **40** 2973
[26] Hosanpoor M, Aliofkhazraei M and Delavari H 2015 *Proc. Mater. Sci.* **11** 320
[27] Hasnidawani J N, Azlina H N, Norita H, Samat N, Bonnia N N and Surip S N 2017 *Mater. Sci. Forum* **894** 76
[28] Selvam M, Saminathan K, Siva P, Saha P and Rajendran V 2016 *J. Mater. Chem. Phys.* **1** 129
[29] Sherif E-S M and Almajid A A 2011 *Int. J. Electrochem. Sci.* **6** 2131
[30] Subannajui K 2016 *Chem. Commun.* **52** 3195
[31] Vogels M J, Kloprogge T and Geus J W 2005 *J. Colloid Interface Sci.* **285** 86
[32] Brindha R, Karthigai Selvii B and Selvam M 2018 *J. Nanosci. Nanotechnol. App.* **2** 6
[33] Lemoine P, Quinn J P, Maguire P D and McLaughlin J A D 2017 *Carbon* **44** 2617
[34] Newton M C and Warburton P A 2007 *Mater. Today* **10** 50
[35] Shiojini M and Kaito C 1985 *J. Cryst. Growth* **5** 64
[36] Ronning C, Shang N G, Gerhards I and Hofsass H 2005 *J. Appl. Phys.* **98** 34307
[37] Wu L, Wu Y, Shi Y and Wei H 2006 *Rare Metals* **25** 68
[38] Raji R and Gopchandran K G 2017 *J. Sci.: Adv. Mater. Devices* **2** 51
[39] Kishore Kumar K, Brindha R, Nandhini M, Selvam M, Saminathan K and Sakthipandi K 2019 *Ionics* **1**, https://doi.org/10.1007/s11581-019-02924-7
[40] Elangovan N 2018 *J. Surf. Sci. Nanotech.* **16** 5